Supplementary Material
Zircon (U-Th)/He (ZHe) thermochronometry

Zircon single crystals were processed at the Dalhousie Noble Gas Extraction Laboratory (Halifax, Canada) for (U-Th)/He dating. They were analyzed following the methods of Reiners et al. (2004; 2005), in parallel with Fish Canyon Tuff standards. Zircon crystals were measured and observed under binoculars to avoid any inclusion and fracture, before being packed into a Nb foil envelope. ^{4}He was then extracted from each aliquot in an in-house built He extraction line with successive 15-min-heatings under a focused beam of a 45 W diode laser (1250 °C), until ^{4}He yields were under 1% of total. After adding a known amount of purified ^{3}He spike, ^{3}He/^{4}He ratios were measured with a Pfeiffer Vaccuum Prisma quadrupole mass spectrometer. Typical 1σ errors are in range of 1.5–2%. Fish Canyon Tuff (FTC) zircon standards were included to ensure the accuracy, reproducibility, and reliability of the data. After He extraction, zircons were dissolved in high-pressure dissolution vessels with concentrated HF and HNO_3 at 200 °C for 96 h. Prior to dissolution, samples were spiked with mixed ^{235}U, ^{230}Th, and ^{149}Sm spikes. Isotopic ratios were measured with iCAP Q inductively coupled plasma mass spectrometry (ICP-MS). Additional blank analyses controlled the analytical accuracy. The raw data were reduced using a Helios software package.

ZHe ages for the Chaltén Plutonic Complex (Fitz Roy massif) are relatively similar to AHe ages presented in this study (Tables 1-2, Fig. 5a). Following the recent studies of Gérard et al. (2022) and Gautheron et al. (2020; 2022), we propose that such age similarity between the ZHe and the AHe systems result from the low α-dose in the zircon crystals, calculated between 6×10^{15} and 5.3×10^{16} (α/g) (Table S2), and linked with a low ^{4}He retention. The α-dose is the total radiation damage accumulated in the crystal lattice, and depends on the age-effective uranium concentration, eU (Table S2), and the time since the crystal began to accumulate damage. The low radiation damage and associated low ^{4}He retention in the zircon crystals of the FzR is most probably explained by the young emplacement age of the Chaltén Plutonic Complex (12.5±0.1 Ma; Ramírez de Arellano et al., 2012). In the following, we estimate the changes in He retention for zircon crystals by calculating the impact of low α-dose on He diffusivity in zircon, which we subsequently relate to the effective closure temperature, T_c, of the ZHe system (Dodson, 1979; Gautheron et al., 2020; 2022; Gérard et al., 2022) (Table S2). We calculate the initial diffusion coefficient D_0 as a function of the damage fraction (f), estimated in terms of α-dose normalized to the total number of atoms in

1g of zircon (Nasdala et al., 2001) and the diffusion coefficient for a zero-damage crystal (1.6 $\times 10^{-7}$ m^2/s, Table 4 in Gautheron et al., 2020). Typical damage fraction for low-damaged zircon will be in the 0.01 to 1 % range. With time, damage content in zircon will increase and the damage fraction will be higher (Gautheron et al., 2020). The activation Energy, E_a, was estimated relative to the α-dose as well with a similar value of 133 kJ/mol for all zircon crystals, as an intermediate value (Fig. 8 of Gautheron et al., 2020) for young zircons with α-dose in the order of 10^{15} and 10^{16}. For inverse QTQt thermal modeling, instead of using an existing model for the He diffusion, we input the activation energy, E_a, and the calculate diffusion coefficient D_0 as shown in Table S2. The resulting T_c between 87 and 108 °C, and the α-dose between 6×10^{15} and 5.3×10^{16} (α/g) of the zircon crystals of the Chaltén Plutonic Complex can help to fill current gaps in our knowledge about low α-dose zircon behaviour, since few studies recognized natural examples with this kinetic behaviour (Gérard et al, 2022).

Apatite (U-Th)/He (AHe) and $^4He/^3He$ thermochronometry

For TdP AHe data, single-crystal aliquots of apatite were wrapped in Pt or Nb foils and degassed by laser heating. At the University of Arizona and the Berkeley Geochronology Center, ^4He abundances were measured using ^3He isotope dilution and quadrupole mass spectrometry (House et al., 2000). Net signal intensities were interpolated to the inlet time of the gas into the mass spectrometer, and then compared to the corresponding mean signal from reference gas aliquots of known absolute amounts analyzed by the same procedure. Degassed aliquots were then dissolved and U, Th and Sm concentrations were measured by isotope dilution using ICP-MS.

For FzR AHe data, individual apatite crystals were encapsulated in Pt tubes before heating under high vacuum conditions at high temperature (1050±50°C using an infrared diode laser) twice for 5 min at GEOPS laboratory (Université Paris-Saclay, France). The released ^4He gas was mixed with a known amount of ^3He, purified, and the gas was analyzed using a Prisma Quadrupole. The ^4He content was determined by isotope dilution method. Subsequently, apatite crystals were dissolved in 100 µL of HNO_3 5 N solution containing known amount of ^{235}U, ^{230}Th, ^{149}Sm, and ^{42}Ca. The solution was heated at 70°C during 3 h and after a cooling time, 900 µL of distilled water was added. The final solution was analyzed using an ELEMENT XR ICP-MS and the ^{238}U, ^{230}Th, and ^{147}Sm concentrations and apatite weight (using the Ca content) were determined following the methodology proposed by

Evans et al. (2005). More details about the analytical procedure can be found in Gautheron et al. (2021).

Durango apatite crystals were also analyzed during the same period to ensure the data quality. Replicate analyses of Durango apatite yielded a <5% reproducibility compared to the reference age. An α-ejection correction was applied to calculate the (U-Th)/He (AHe) age (Farley et al., 1996). The one-sigma error on each AHe age amounts to around 8%, reflecting the analytical error and the uncertainty on the F_t ejection factor correction. Sample locations and details, as well as all individual AHe ages, crystal characteristics and mean ages appear in Tables 2 and 3.

In $^4He/^3He$ thermochronometry (Shuster and Farley, 2004) the natural spatial distribution of radiogenic ^4He is constrained by stepwise degassing and $^4He/^3He$ analysis of a sample containing synthetic, homogeneously distributed, proton-induced ^3He. Approximately 50 mg of apatite crystals were packaged into Sn foil and exposed to $\sim 5 \times 10^{15}$ protons cm^{-2} with incident energy of ~220 MeV over a continuous ~5-hour period at the Francis H. Burr Proton Therapy Center (Boston, USA). Euhedral crystals free of visible mineral inclusions were selected using the above criteria; crystal dimensions were measured using a calibrated binocular microscope. Individual crystals were then sequentially heated in multiple steps under ultra-high vacuum using a feedback-controlled 70-W diode laser, with temperature measured with a coaxially aligned optical pyrometer at the Noble Gas Thermochronometry Laboratory (Berkeley Geochronology Center, USA). The molar ^3He abundance and the $^4He/^3He$ ratio were measured for each heating step using calibrated pulse-counting sector-field mass spectrometry and corrected for blank contributions to ^3He and ^4He (uncertainties in blank corrections are propagated into ratio uncertainties). All stepwise $^4He/^3He$ degassing data are given in Tables S1 a,b. A few heating steps yielded $^4He/^3He$ ratios that plot well outside analytical uncertainty relative to contiguous heating steps and therefore result in evolving ratios that do not monotonically increase over the course of certain stepped heating analyses. Potential explanations for these anomalous ratios include: (i) inaccuracy in the ^4He blank correction for a particular heating step, or (ii) small cracks within the crystal that were not visible via optical microscopy. To minimize the influence of anomalous $^4He/^3He$ ratios and simultaneously place some constraint on the most likely cooling scenarios, these data (open gray boxes in Fig. 9a,c) were excluded from the calculation of misfit statistics. Somehow, inclusion of these data would result in lower levels of confidence in the excluded cooling paths, with most of the constraint therefore derived from the AHe age alone.

Supplementary Figures

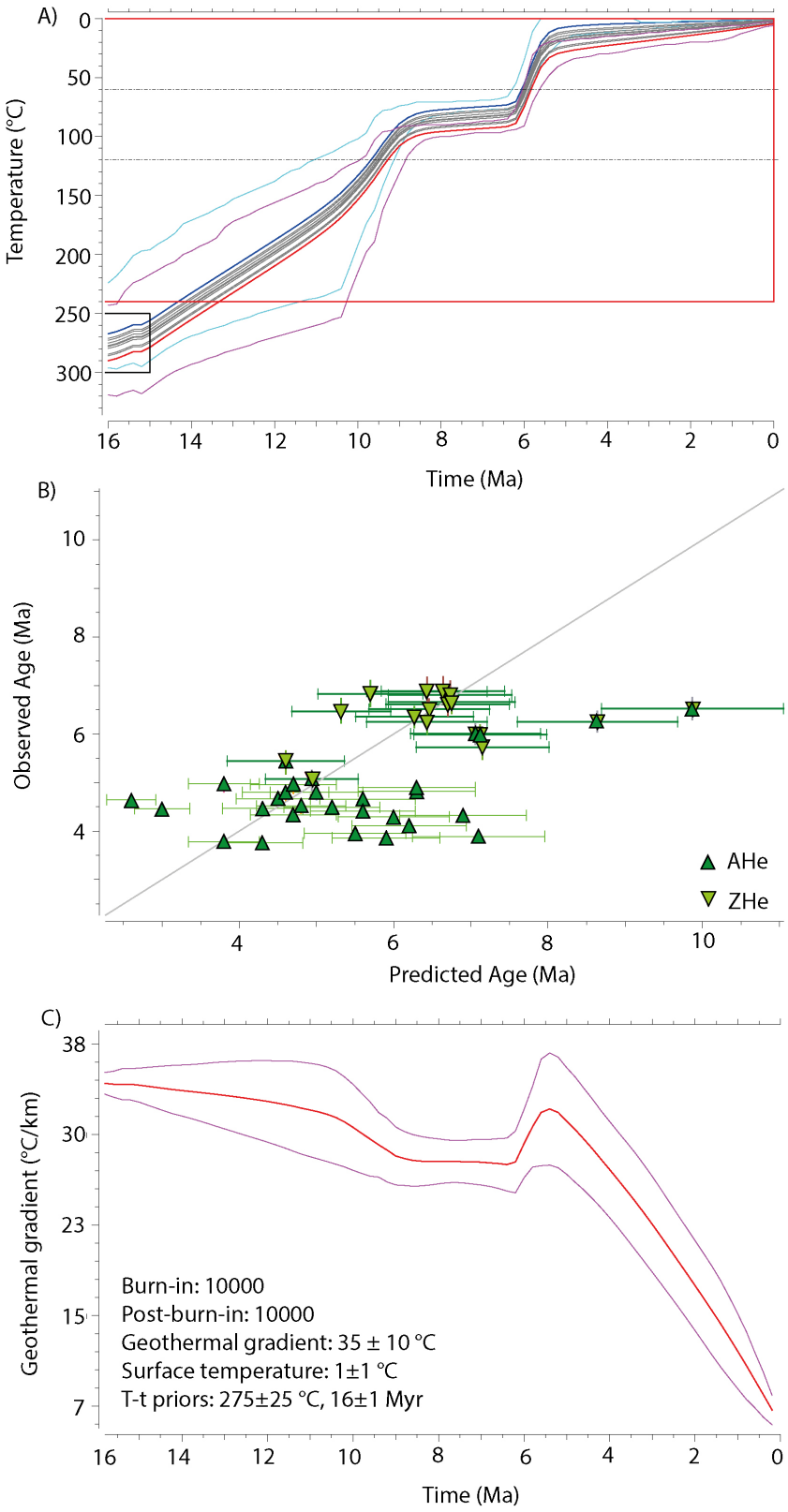

Figure S1 - QTQt thermal modeling outputs for the FzR massif. A) Expected (weighted mean) T-t model based on AHe and ZHe data presented in Fig. 5a. Red and blue lines correspond to the output thermal history for the highest and lowest elevation samples, respectively. Gray lines are output thermal histories of the intermediate samples. The cyan and magenta lines bound the 95% confidence interval of the expected model for the lowest and the highest elevation samples, respectively. The black box indicates the initial thermal constraints, and the red box is representing general T-t priors. B) Observed vs. predicted age diagram with single-crystal AHe (green triangles) and ZHe (downward green triangles) uncorrected ages. C) The Predicted geothermal gradient (red line) and 95% of confidence interval (magenta lines) from inverse thermal modeling. Note that the late-stage evolution is reflecting the gradual transition form geothermal (35±10°C/km) to atmospheric (lapse rate, 6±2°C/km) gradient during rock exhumation towards the surface.

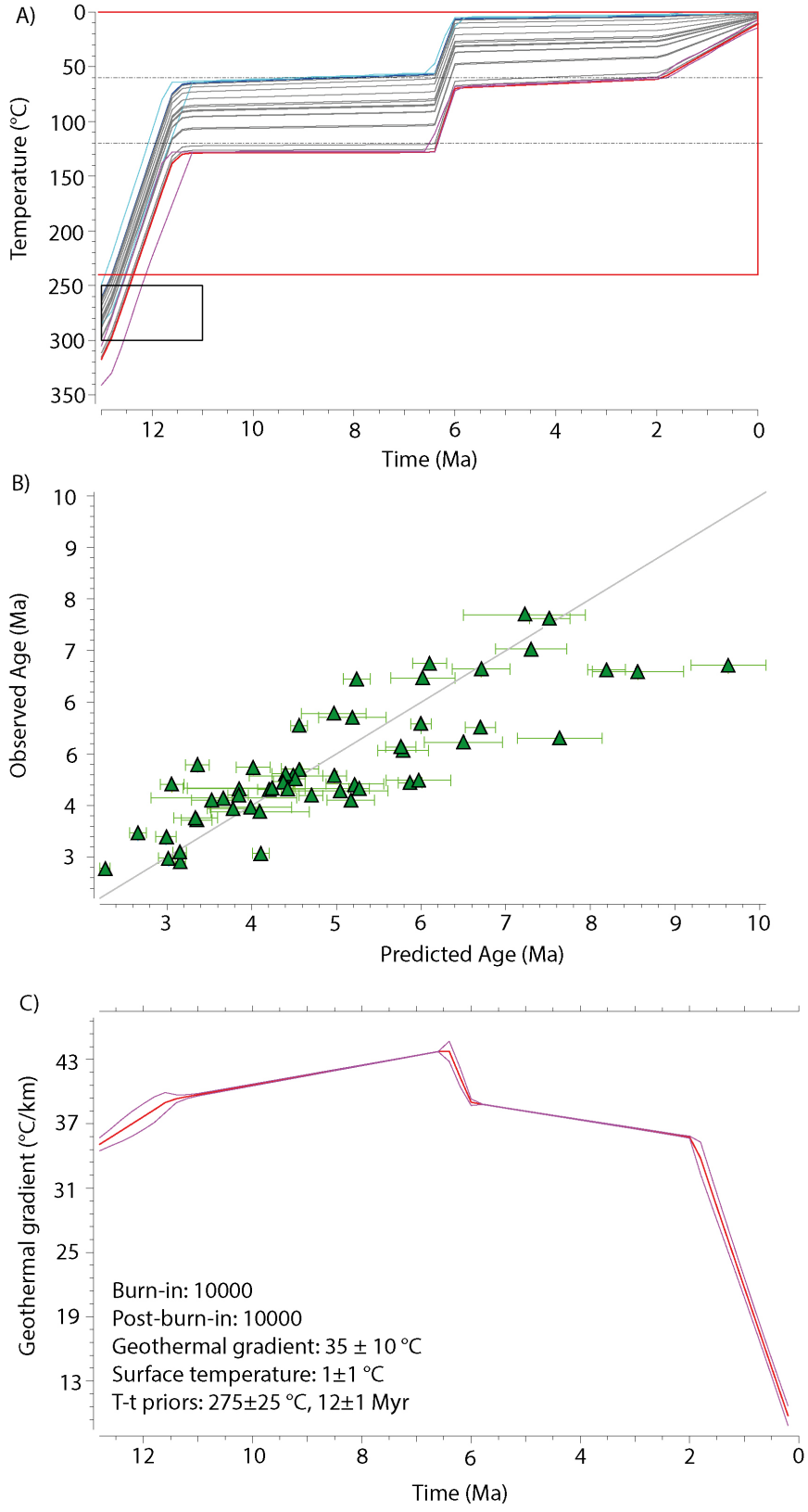

Figure S2 - QTQt thermal modeling outputs for the TdP massif, Central sector. A) Expected (weighted mean) T-t model based on AHe data presented in Fig. 5b. Red and blue lines correspond to the output thermal history for the highest and lowest elevation samples, respectively. Gray lines are output thermal histories of the intermediate samples. The cyan and magenta lines bound the 95% confidence interval of the expected model for the lowest and the highest elevation samples, respectively. The black box indicates the initial thermal constraints, and the red box is representing general T-t priors. B) Observed vs. predicted age diagram with single-crystal AHe (green triangles) uncorrected ages. C) The Predicted geothermal gradient (red line) and 95% of confidence interval (magenta lines) from inverse thermal modeling. Note that the late-stage evolution is reflecting the gradual transition form geothermal (35±10°C/km) to atmospheric (lapse rate, 6±2°C/km) gradient during rock exhumation towards the surface.

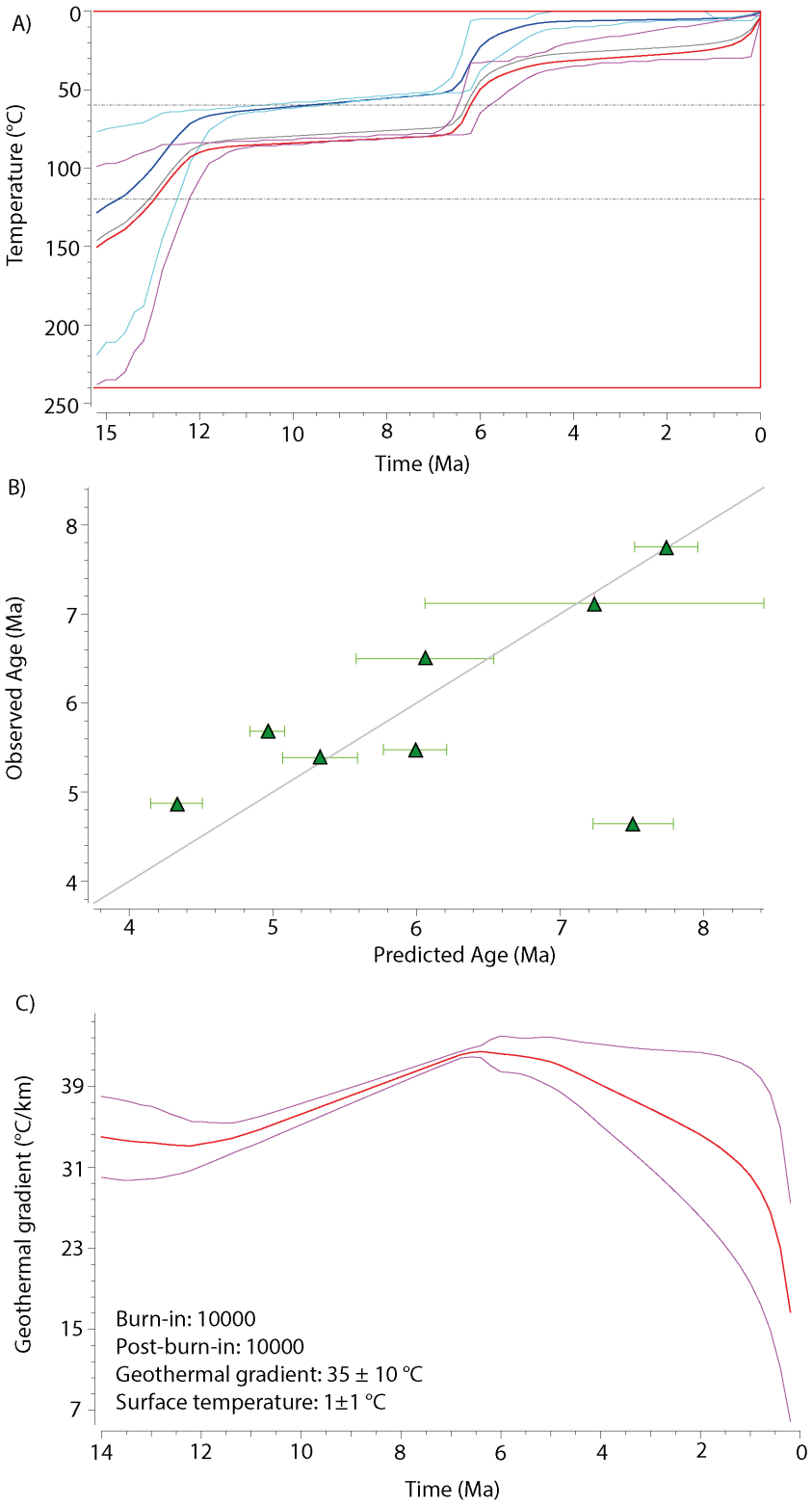

Figure S3 - QTQt thermal modeling outputs for the TdP massif, West sector. A) Expected (weighted mean) T-t model based on AHe data presented in Fig. 5 b. Red and blue lines correspond to the output thermal history for the highest and lowest elevation samples, respectively. Gray lines are output thermal histories of the intermediate samples. The cyan and magenta lines bound the 95% confidence interval of the expected model for the lowest and the highest elevation samples, respectively. The black box indicates the initial thermal constraints, and the red box is representing general T-t priors. B) Observed vs. predicted age diagram with single-crystal AHe (green triangles) uncorrected ages. C) The Predicted geothermal gradient (red line) and 95% of confidence interval (magenta lines) from inverse thermal modeling. Note that the late-stage evolution is reflecting the gradual transition form geothermal (35±10°C/km) to atmospheric (lapse rate, 6±2°C/km) gradient during rock exhumation towards the surface.

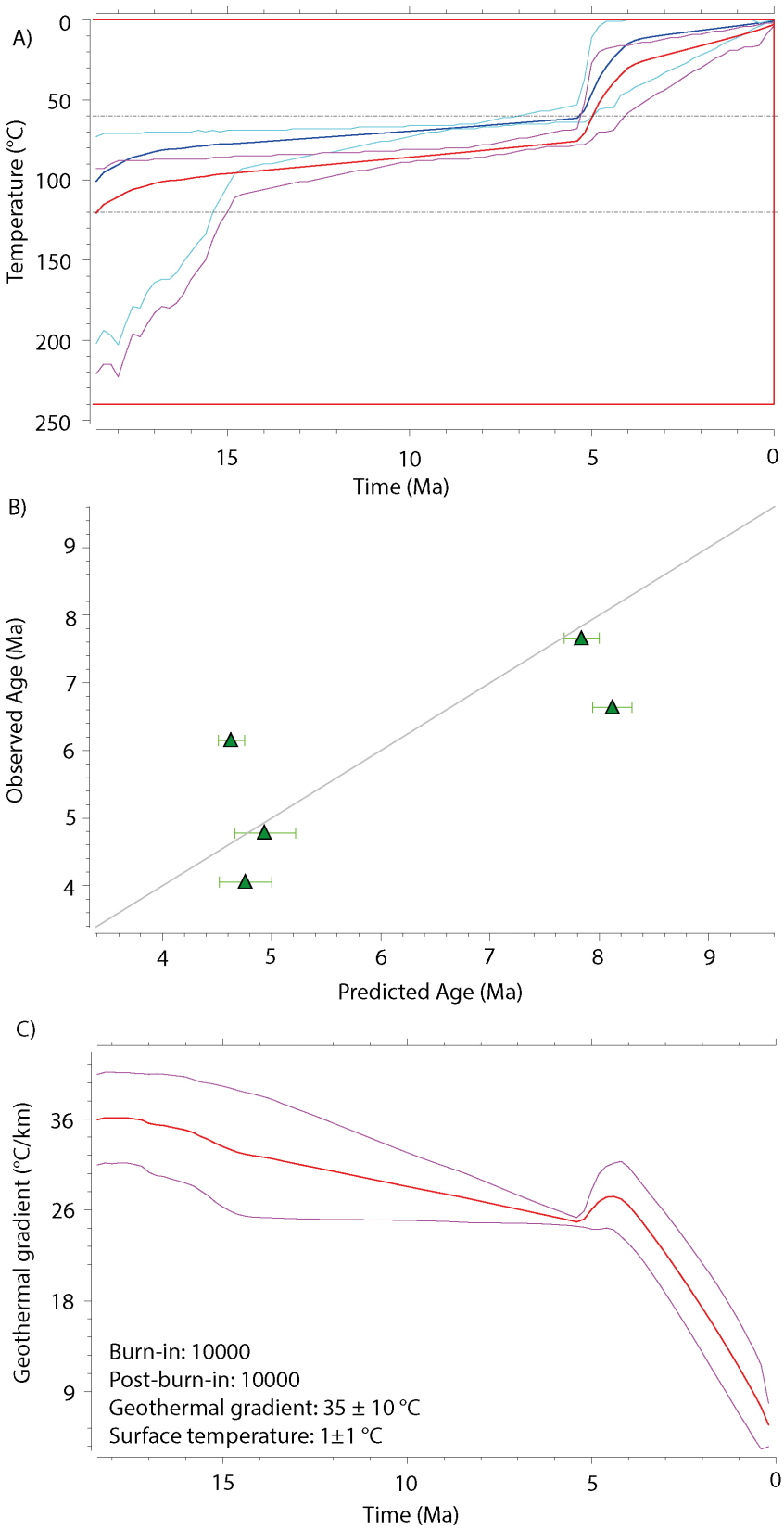

Figure S4 - QTQt thermal modeling outputs for the TdP massif, North sector. A) Expected (weighted mean) T-t model based on AHe data presented in Fig. 5b. Red and blue lines correspond to the output thermal history for the highest and lowest elevation samples, respectively. Gray lines are output thermal histories of the intermediate samples. The cyan and magenta lines bound the 95% confidence interval of the expected model for the lowest and the highest elevation samples, respectively. The black box indicates the initial thermal constraints, and the red box is representing general T-t priors. B) Observed vs. predicted age diagram with single-crystal AHe (green triangles) uncorrected ages. C) The Predicted geothermal gradient (red line) and 95% of confidence interval (magenta lines) from inverse thermal modeling. Note that the late-stage evolution is reflecting the gradual transition form geothermal (35±10°C/km) to atmospheric (lapse rate, 6±2 °C/km) gradient during rock exhumation towards the surface.

Supplementary Tables

Table S1a. Stepwise $^{4}He/^{3}He$ degassing data for Torres del Paine sample 04-JM-90a.

04-JM-90a (758 m)						
Step	Temperature* (°C)	Duration (hours)	^{3}He ($\times 10^{6}$ atoms)	(±) ($\times 10^{6}$ atoms)	$^{4}He/^{3}He$	(±)
1	210	0.2	0.006	0.001	2058.40	6513.08
2	225	0.5	0.049	0.004	391.81	303.77
3	260	0.38	0.096	0.007	437.33	163.28
4	300	0.51	0.444	0.022	376.70	39.49
5	300	0.66	0.233	0.014	589.97	82.25
6	310	0.66	0.287	0.017	612.92	70.86
7	330	0.46	0.297	0.017	746.94	78.31
8	340	0.45	0.349	0.019	815.25	72.20
9	350	0.48	0.377	0.020	965.31	77.20
10	350	0.66	0.421	0.021	1054.30	75.91
11	370	0.53	0.503	0.024	1233.72	76.86
12	400	0.48	0.723	0.029	1537.27	72.97
13	410	0.5	0.799	0.031	1542.67	69.22
14	420	0.56	0.700	0.029	1902.99	89.92
15	440	0.63	0.864	0.032	1971.67	80.89
16	475	0.5	0.803	0.031	2183.20	94.58
17	500	0.5	0.590	0.026	2101.45	110.96
18	600	0.5	0.489	0.023	2391.61	141.96
19	700	0.5	0.006	0.001	9494.85	26907.71
20	900	0.5	0.010	0.001	659.04	1768.82

Notes. *Temperatures of these analyses are approximate, and controlled to ±50 °C.
BDL: Below Detection Limit.
Effective model: a = 59.9 μm; U = 21.0 ppm; Th = 27.1 ppm.
Single-crystal replicates: (U-Th)/He age = 6.60±1.22 Ma; mean replicates a = 60.3 μm.

Table S1b. Stepwise $^{4}He/^{3}He$ degassing data for Torres del Paine sample 13-TP-26a.

13-TP-26a (206 m)						
Step	Temperature* (°C)	Duration (hours)	^{3}He ($\times 10^{6}$ atoms)	(±) ($\times 10^{6}$ atoms)	$^{4}He/^{3}He$	(±)
1	210	0.2	0.010	0.001	BDL	BDL
2	225	0.5	0.137	0.010	9.68	38.31
3	260	0.38	0.299	0.018	6.56	19.96
4	300	0.51	0.947	0.035	17.33	4.95
5	300	0.66	0.657	0.029	24.36	11.64
6	310	0.66	0.570	0.026	38.46	11.12
7	330	0.46	0.617	0.028	49.51	9.70
8	340	0.45	0.674	0.029	50.97	8.84
9	350	0.48	0.766	0.031	56.26	7.51
10	350	0.66	0.708	0.030	69.94	8.53
11	370	0.53	0.813	0.032	74.44	9.58
12	400	0.48	1.373	0.043	74.09	5.37
13	410	0.5	1.318	0.042	77.77	5.66
14	420	0.56	1.380	0.043	82.26	5.62
15	440	0.63	1.850	0.051	81.79	3.72
16	475	0.5	2.793	0.063	87.70	3.39
17	500	0.5	2.323	0.057	102.05	3.94
18	600	0.5	2.594	0.061	122.40	4.74
19	700	0.5	0.135	0.010	307.72	63.39
20	900	0.5	0.053	0.005	670.05	254.61

Notes. *Temperatures of these analyses are approximate, and controlled to ±50 °C.
BDL: Below Detection Limit.
Effective model: a = 61.0 μm; U = 12.2 ppm; Th = 52.6 ppm.
Single-crystal replicates: (U-Th)/He age = 4.20±0.94 Ma; mean replicates a = 60.8 μm.

Table S2. Calculations of the radiation damage, kinetic He diffusion parameters and closure temperature of the ZHe system in the Fitz Roy massif samples in a scenario in which the low α-dose is linked to the relatively young age of the pluton of 12.5±0.1 Ma (Ramírez de Arellano, 2012). The α-dose, f and D_0 estimates were calculated based in Gautheron et al. (2020), using a common activation energy (E_a value of 133 kJ/mol (see text for details), and the Tc estimates were based in Dodson (1979).

	Corr. Age ± 1σ (Ma)	**eU (ppm)**	**α-dose (α/g)**	**f (%)**	**D_0 (m^2/s)**	**T_c (°C)**
zFZR3-1	8.24	226.86	6.11797E+15	0.2	0.00008	90.6
zFZR3-2	8.47	307.51	8.51577E+15	0.2	0.00008	91.16
zFZR3-3	8.24	542.86	1.4624E+16	0.6	2.66667E-05	99.15
zFZR3-4	8.50	548.91	1.52487E+16	0.6	2.66667E-05	99.15
zFZR3-5	8.69	577.81	1.64245E+16	0.6	2.66667E-05	98.83
FZR3	8.43 ±0.19					
zFZR4-1	8.30	403.74	1.09639E+16	0.5	0.000032	95.7
zFZR4-3	8.26	334.71	9.03723E+15	0.2	0.00008	90.3
zFZR4-4	7.14	1204.03	2.81155E+16	1	0.000016	100.69
zFZR4-5	7.31	769.46	1.83981E+16	0.8	0.00002	101.56
FZR4 AV	7.75 ±0.61					
zFZR5-1	8.66	978.23	2.77215E+16	1	0.000016	103.44
zFZR5-2	9.54	293.70	9.1662E+15	0.3	5.33333E-05	91.26
zFZR5-3	6.22	484.01	9.85664E+15	0.2	0.00008	87.73
zFZR5-4	9.72	584.72	1.8603E+16	0.8	0.00002	98.09
zFZR5-5	6.11	591.26	1.18174E+16	0.5	0.000032	94.26
FZR5 AV	8.05 ±1.77					
zFZR6-1	12.87	1244.72	5.23982E+16	2	0.000008	108.37
zFZR6-2	11.59	1331.37	5.05061E+16	2	0.000008	106.56
zFZR6-3	9.58	1087.78	3.40949E+16	1.5	1.06667E-05	103.3
zFZR6-4	6.68	435.66	9.51279E+15	0.2	0.00008	87.38
FZR6 AV	10.2 ±2.70					

Notes. eU is the effective uranium concentration, f is the damage fraction, D_0 is the initial diffusion coefficient, and T_c is the effective closure temperature of the ZHe system.